NASA TECHNICAL NOTE
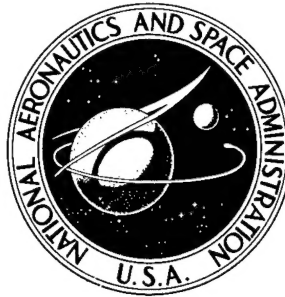
NASA TN D-5135

NASA TN D-5135

AMPTIAC

CRATER CHARACTERISTICS OF 11 METAL ALLOYS
UNDER HYPER-VELOCITY IMPACT INCLUDING
EFFECTS OF PROJECTILE DENSITY
AND TARGET TEMPERATURE

by

Nestor Clough and Seymour Lieblein
Lewis Research Center

and

A. R. McMillan
General Motors Corporation

NATIONAL AERONAUTICS AND SPACE ADMINISTRATION • WASHINGTON, D. C. • APRIL 1969

CRATER CHARACTERISTICS OF 11 METAL ALLOYS UNDER HYPER-VELOCITY IMPACT INCLUDING EFFECTS OF PROJECTILE DENSITY AND TARGET TEMPERATURE

By Nestor Clough and Seymour Lieblein

Lewis Research Center
Cleveland, Ohio

and

A. R. McMillan

General Motors Corporation
Warren Research Laboratories

APRIL - 1969

NATIONAL AERONAUTICS AND SPACE ADMINISTRATION

ABSTRACT

An experimental research program was conducted to determine the cratering characteristics resulting from the impact of high velocity projectiles in 11 different metal alloys. Spherical Pyrex, aluminum, steel, nylon, and Inlyte projectiles were accelerated to velocities from 4.88 to 8.35 kilometers per second and impacted against thick flat plate targets at room and elevated temperatures. Targets impacted were aluminum alloys 2024-T6, 7075-T6, and 356-T51, columbium - 1 percent zirconium, tantalum, vanadium, molybdenum-TZM, A-286, Inconel-718, 316 stainless steel, and L-605. Correlations were determined for the effects of projectile density and target temperature on the cratering characteristics of these materials.

CRATER CHARACTERISTICS OF 11 METAL ALLOYS UNDER

HYPER-VELOCITY IMPACT INCLUDING EFFECTS OF

PROJECTILE DENSITY AND TARGET TEMPERATURE

by Nestor Clough, Seymour Lieblein, and A. R. McMillan*

Lewis Research Center

SUMMARY

An experimental research program was conducted to determine the cratering characteristics resulting from the impact of high velocity spherical projectiles in 11 different metal alloys. The experimental program was performed under NASA contract on a ballistics range facility of the General Motors Corporation, Defense Research Laboratories, Santa Barbara, California. Spherical Pyrex, aluminum, steel, nylon, and Inlyte projectiles of nominally 2.38, 3.18, or 3.68 millimeters in diameter were accelerated to velocities from 4.88 to 8.35 kilometers per second and impacted against thick-flat plate targets at room and elevated temperatures in an evacuated chamber. Targets impacted included the aluminum alloys 2024-T6, 7075-T6, and 356-T51, columbium - 1 percent zirconium, tantalum, vanadium, molybdenum-TZM, A-286, Inconel-718, 316 stainless steel, and L-605.

Correlations were determined for the effects of projectile density and target temperature on the cratering characteristics of these materials. A general relation was defined for predicting crater depth based on target room-temperature properties.

INTRODUCTION

The use of large space vehicles on extended missions has introduced the possibility of damaging impacts by meteoroids upon the vulnerable components of vehicles. These impacts could impair mission success if appropriate protective measures are not taken. The description of the meteoroid population most often applied in space vehicle compo- nent design is that given by Whipple (ref. 1). Modifications to the environment of

---

*General Motors Corporation, Warren Research Laboratories.

reference 1 are sometimes applied as suggested by reference 2. By utilizing these flux estimates and typical space-vehicle vulnerable areas and mission times, it is determined in reference 2 that large space vehicle components must be protected against impacts by meteoroids with masses in the range of 10^{-2} to 10^{-4} grams impacting at velocities of the order of 20 kilometers per second.

The study of the phenomena of such high-speed impacts has been pursued on both the theoretical and experimental level. These studies have provided a general description of the processes of hypervelocity impact. Early theoretical treatments of the high-speed impact process have been carried out by Bjork (ref. 3), Walsh (ref. 4), and Riney (ref. 5). These treatments are hydrodynamic in nature and are based upon the assumption that the early phases of the impact are governed by pressures far in excess of the target and projectile material strengths, and thus target and projectile strength effects can be ignored. Because these calculations are inviscid, none of the treatments carry the processes to completion, that is, the point at which all flow of material has ceased and no further deformation takes place. Thus it was not possible to theoretically predict the complete high velocity impact process.

Recently, some encouraging success has been obtained with thick-place cratering calculations for targets and projectiles of the same material (ref. 6). The calculations compared the dynamic pressure in the region surrounding the forming crater to the residual yield strength of the target material in the wake of the shock. When the two were equal, the cratering process was stopped. The explicit prediction of crater depths for 2024-T6 and 2014-T6 aluminum targets and projectiles using the above criterion for crater formation was found to be in excellent agreement with experimental data at 7.35 kilometers per second impact velocity (ref. 6).

The experimental study of high-speed impact has advanced a great deal in recent years in the areas of velocity capability and projectile sophistication. However, experimental velocities obtainable with discrete, well-defined projectiles are generally limited to less than 10 kilometers per second. In order to make confident predictions of meteoroid impact damage, it is necessary to perform experiments within the experimental limitations and extrapolate the results to the meteoroid range with guidance from the theoretical results.

An experimental hypervelocity impact program was initiated by the NASA Lewis Research Center with the overall objective of determining and predicting the damage characteristics of specific materials and configurations when subjected to high velocity impacts. The materials and configurations tested were intended to be specifically applicable to space waste-heat radiator design. Previous results from this program can be found in references 7 to 9. Results presented in references 7 and 8 characterize the various types of damage that exist in tubes subjected to high velocity impacts. Results of reference 9 give insight into the usefulness of using the explosive technique

2

for producing high velocity projectiles for impact studies. The results of reference 9 generally corroborate the peak axial pressure predictions of the theoretical analyses of reference 10.

It was found early in the overall hypervelocity impact program (ref. 7), that data on each specific armor material were required to make use of existing empirical relations for crater predictions. The existing correlations contained coefficients which were found to be functions of the particular material impacted and the conditions of impact. Further impact tests were therefore conducted on a number of specific metal alloys potentially applicable for space radiator armor use to provide data for correlating theoretical and experimental results, and to provide insight into the general cratering process. These hypervelocity impacts were performed on eleven different materials in the form of thick (semi-infinite) flat plates. Variations of impact velocity, projectile material and density, and target temperatures were investigated. The target materials investigated included several aluminum alloys, A-286, Inconel-718, columbium - 1 percent zirconium, tantalum, molybdenum-TZM, 316 stainless steel, L-605, and vanadium.

Reported herein are the results of this experimental investigation. All the impact work was conducted under NASA contract at the ballistics range facilities of the General Motors Corporation, Defense Research Laboratories, Santa Barbara, California. Presented are the impact data, including conditions of impact and cratering results, and the effects of variation in projectile velocity and density and of target temperature on cratering characteristics. Also included is a presentation of cratering equations dependent on room-temperature target material properties which will successfully predict crater depths at elevated temperatures.

DESCRIPTION OF EXPERIMENTS

The experiments were performed with projectiles of Pyrex, aluminum, nylon, Inlyte, and steel launched from a light-gas gun which is fully described in reference 11. The ballistics range consists of a 30-caliber accelerated reservoir light-gas gun, a 6-meter free-flight range, and an evacuated impact chamber. The projectiles were launched and impacted at velocities nominally in the range of 7.32 kilometers per second, with special tests for variation in impact velocity from 4.88 to 8.35 kilometers per second.

The targets were thick circular disks or squares cut from commercially available single bars, or from several bars or billets from the same heat. In this way, variations in material mechanical properties due to differences between heats was held to a minimum. The thicknesses of the targets were chosen to be great enough to prevent

TABLE I. - IMPACT VARIABLE

Target material	Target temperature, K	Projectile velocity, km/sec	Projectile diameter (mm) and material
Tantalum	RT, 977, 1365	Nominally 7.32	3.18 Pyrex
A-286	RT, 977		
Inconel-718	RT, 977		
7075-T6 Aluminum	RT, 481, 644		3.18 Pyrex and 3.18 2017 aluminum
2024-T6 Aluminum	RT,		2.38 Pyrex, 3.18 2017 aluminum and 3.18 steel
356-T51 Aluminum	RT, 481, 644	5.00 to 8.35	2.38 and 3.18 Pyrex, 3.18 2017 aluminum, and 3.18 nylon
Columbium - 1 percent zirconium	RT, 644, 977, 1365	4.88 to 7.62	3.18 and 2.38 Pyrex, 3.18 2017 aluminum, 3.18 nylon and 3.18 steel
TZM - molybdenum	RT, 1365	Nominally 7.32	3.18 Pyrex
Vanadium	RT, 977, 1365		
L-605	RT, 977		
316 Stainless steel	RT, 644, 977		3.18 and 2.38 Pyrex, 3.18 2017 aluminum, 3.18 nylon, 3.18 steel, and 3.68 Inlyte

TABLE II. - CALCULATED AVERAGE (SPHERICAL)

PROJECTILE DENSITY

Projectile diameter and material	Density, g/cm^3
2.38-mm Pyrex	2.31
3.18-mm Pyrex	2.46
3.18-mm Nylon	1.13
3.18-mm Aluminum	2.79
3.18-mm Steel	7.81
3.68-mm Inlyte	.749

any deformation of the rear surface so that the crater formation would not be influenced by the thin or finite-target effect (ref. 8).

For the impacts performed at room temperature the targets were mounted directly in the impact chamber. For those tests in which the targets were heated to temperatures up to 977 K, the targets were mounted in resistance heaters which in turn were mounted within the impact chamber. The targets impacted at 1365 K were heated in an induction heater coil within the impact chamber. The temperature of the heated targets was determined by means of thermocouples imbedded within the targets with the thermocouple output monitored by a potentiometer. In all cases the targets were positioned such that the target face was normal to the impacting projectile flight line.

All impacts were performed under partial vacuum conditions. The unheated targets were in a 30 millimeters of mercury nitrogen-air atmosphere, and the heated targets were in a 30 millimeters of mercury helium atmosphere. Results of the tests were the measurements of crater dimensions after impact. The depth of the crater P_∞ was measured with respect to the original target surface, and the measurement of crater diameter D_∞ was also based on the plane of the original target surface. A list of symbols used in this report is included in the appendix.

A total of 61 experiments were performed utilizing 11 target materials, 5 projectile materials, and 3 projectile sizes. Table I presents the various impact variables covered in these tests. Targets were impacted at a nominal projectile velocity of 7.32 kilometers per second, except for cast aluminum (356-T51) at 481 K and columbium - 1 percent zirconium at room temperature for which 3.18 millimeters of Pyrex projectiles were impacted over a range of velocities from around 5.0 to 8.35 kilometers per second.

Table II presents the calculated average densities of the spherical projectiles used in the program. These densities were determined from measurements of weight and diameter for all the projectiles used.

RESULTS AND DISCUSSION

The quantitative results of the experiments are presented in table III. The crater depth and diameter are given along with a description of the projectile, that is, size, mass, material, and impact velocity. Several calculated parameters are also included in the table. The targets are identified by material and temperature. The results of these experiments are described below in groupings in which only 1 parameter was varied at a time.

TABLE III. - ORIGINAL AND REDUCED DATA

Shot	Target Material	Temperature, K	Density, ρ_t, g/cm³	Modulus of elasticity, E_t, dyne/cm²	Projectile Material	Velocity, V, km/sec	Diameter, d, mm	Mass, m, g	Density, ρ_p, g/cm³	Crater Depth, P_∞, cm	Crater Diameter, D_∞, cm	Ratio of crater depth to projectile diameter, P_∞/d	Ratio of crater depth to crater diameter, P_∞/D_∞	Density ratio, $\left(\dfrac{\rho_p}{\rho_t}\right)^{2/3}$	$\left(\dfrac{v}{\sqrt{E_t/\rho_t}}\right)^{2/3}$	Ratio of target absolute temperature to target absolute melting temperature, T/T_m
340	Molybdenum	294.1	10.2	33.8×10¹¹	Pyrex	7.75	3.18	0.0412	2.46	0.305	0.787	0.96	0.388	0.387	1.22	0.102
547	Molybdenum	1365	10.2	28.2	→	7.62	→	.0421	→	.444	1.07	1.40	.417	.387	1.28	.473
337	316 Stainless steel	294.1	8.0	19.9	→	7.38	→	.0424	→	.386	1.07	1.22	.362	.456	1.31	.176
338	→	644	→	17.0	→	7.53	→	.0412	→	.450	1.07	1.41	.422	→	1.39	.385
339	→	977	→	14.1	→		→	.0412	→	.483	1.14	1.59	.422	→	1.475	.584
1271	→	294.1	→	19.9	→	7.62	→	.0410	→	.391	.864	1.23	.454	→	1.33	.176
1270	→	977	→	14.1	→	7.60	→	.0409	→	.482	1.17	1.52	.413	→	1.475	.584
487	→	294.1	→	19.9	Inlyte	7.48	2.38	.0156	2.31	.325	.686	1.36	.475	.437	1.34	.176
1311	→	→	→	→			3.68	.0195	.749	.234	.660	.635	.354	.206	1.34	→
1078	→	→	→	→	Nylon		3.18	.0199	1.13	.262	.660	.82	.396	.271	1.323	→
1199	→	→	→	→	Nylon	6.99	→	.0189	1.13	.241	.610	.76	.396	.271	1.264	→
1269	→	→	→	→	Nylon	7.38	→	.0194	1.13	.241	.660	.76	.365	.271	1.31	→
350	→	→	→	→	Aluminum	7.71	→	.0468	2.79	.396	.991	1.25	.400	.496	1.35	→
1272	→	→	→	→	Aluminum	7.41	→	.0468	2.79	.394	.915	1.24	.430	.496	1.316	→
1268	→	→	→	→	Steel	6.21	→	.1315	7.81	.688	1.32	2.17	.522	.985	1.173	→
384	Tantalum	294.1	16.6	19.2	Pyrex	7.84	3.18	.0410	2.46	.307	.864	.97	.356	.280	1.75	.090
385	Tantalum	977	16.6	17.4	→	7.69	→	.0411	→	.361	.965	1.14	.374	.280	1.78	.290
543	Tantalum	1365	16.6	16.4	→	7.77	→	.0411	→	.386	.915	1.22	.423	.280	1.84	.418
1289	A-286	294.1	7.92	19.3	→	7.50	→	.0412	→	.386	.915	1.22	.423	.458	1.32	.173
1262	A-286	977	7.92	14.4	→	7.56	→	.0418	→	.429	.915	1.35	.470	.458	1.49	.575
1290	Inconel-718	294.1	8.23	20.1	→	7.53	→	.0410	→	.366	.864	1.15	.424	.447	1.325	.185
1267	Inconel-718	977	8.23	15.8	→	7.62	→	.0419	→	.450	.965	1.42	.466	.447	1.445	.616
221	7075-T6	294.1	2.79	6.96	→	7.90	→	.0409	→	.790	1.27	2.49	.623	.920	1.356	.324
237	→	481	→	6.35	→	8.05	→	.0413	→	.889	1.60	2.80	.556	.920	1.41	.526
223	→	644	→	5.39	→	7.84	→	.0411	→	.920	1.60	2.90	.574	.920	1.47	.709

The following is a continuation data table (no column headers printed). Values read left-to-right; "→" indicates a continuation/same-as arrow in the original, and "---" indicates dashes as printed.

ID	Material				Material											
239	L-605	294.1	9.15	6.96	Aluminum	8.17	→	.0464	2.79	.803	1.42	2.53	.564	1.00	1.387	.324
1191	L-605	294.1	9.15	23.7	Pyrex	6.31		.0425	2.46	.315	.787	.99	.400	.416	1.086	.175
1192	L-605	294.1	9.15	23.7	→	7.10		.0411	2.46	.305	.787	.96	.388	.416	1.176	.175
1193	L-605	977	9.15	18.3	→	7.25	→	.0423	2.46	.406	.838	1.28	.484	.416	1.304	.581
478	2024-T6	294.1	2.79	7.1	→	7.31	2.38	.0157	2.31	.497	.915	2.09	.544	.882	1.28	.314
898	→	→	→	→	Aluminum	7.90	3.18	.0470	2.79	.679	---	2.13	---	1.000	1.345	→
906					Aluminum	7.53	→	.0473	2.79	.689	---	2.16	---	1.000	1.305	→
1074		977	6.11	13.7	Steel	6.65	→	.1316	7.81	.736	1.40	3.94	.527	.99	1.12	.148
386	Vanadium	→	6.11	13.7	Pyrex	7.69	→	.0414	2.46	.391	1.12	1.23	.35	.546	1.382	.482
389	Vanadium	977	6.11	12.3	→	7.80	3.18	.0411	2.46	.493	1.14	1.55	.431	.546	1.446	.482
548	Vanadium	1365	6.11	10.3	→	7.71	→	.0422	2.46	.586	1.14	1.85	.513	.546	1.492	.689
301	356-T51	294.1	2.79	6.84	→	7.62	→	.0151	2.31	.612	1.02	2.51	.602	.882	1.33	.332
312	→	294.1	→	6.84	→	7.53	→	.0176	2.31	.643	1.07	2.70	.602	.882	1.32	.332
220		481		6.20	→	8.05	→	.0409	2.46	.901	1.42	2.84	.635	.920	1.425	.539
203		644		5.59	→	7.62	→	.0426	2.46	.957	1.83	3.02	.523	.920	1.425	.726
130		644	644	5.59	Aluminum	5.00	→	.0413	→	.813	---	2.56	.658	→	1.075	→
163		→		→	→	5.95	→	.0413	→	.910	1.42	2.86	.694		1.21	→
164				→	→	6.74	→	.0413	→	1.025	1.47	3.22	.655		1.31	→
176		294.1	8.05	6.84	→	7.38	→	.0416	→	1.830	1.80	3.72	---	→	1.394	→
122		→	→	→	Aluminum	8.35	→	.0469	2.79	1.091	---	3.44	---	1.00	1.414	.539
899					Steel	7.86	→	.0470	→	.830	---	2.62	---	→	1.36	→
900					Pyrex	8.05	→	.0473	→	.805	---	2.54	---		1.38	→
907					→	7.53	→	.0473	→	.849	1.37	2.67	.62		1.32	→
908					→	7.71	2.38	.0469	→	.830	1.37	2.62	.605	→	1.34	→
1066			12.4	12.4	Nylon	7.07	2.38	.0190	1.13	.477	1.02	1.51	.47	.547	1.254	.108
1073	Cb – 1 Zr	977			Steel	6.71		.1316	7.81	1.599	1.57	5.03	1.01	.990	1.22	→
101		1365			Pyrex	4.88	3.18	.0422	2.46	.249	---	.78	---	.454	1.16	→
102		294.1			→	6.12	3.18	.0419	→	.333	---	1.05	---	→	1.35	→
103		644			→	7.38	3.18	.0417	→	.396	---	1.25	---	→	1.53	→
96		294.1			→	7.38		.0417	2.31	.329	---	1.35	---	→	1.53	→
353			12.0		Aluminum	7.62		.0416	2.31	.525	1.32	1.66	.399	→	1.57	.352
544			11.9		Nylon	7.71		.0409	2.79	.559	1.35	1.76	.415		1.59	.492
1196		294.1	12.4		Steel	7.50		.0412	1.13	.381	.965	1.20	.395		1.55	.108
320		644	12.2		→	7.56		.0176	7.81	.356	.864	1.49	.412	.434	1.56	.232
1070		294.1	12.4		Aluminum	7.19		.0472	2.31	.396	1.02	1.25	.39	.494	1.505	.108
1071		294.1	12.4		Nylon	7.14		.0198	2.79	.239	.711	.75	.336	.270	1.496	.108
1072		294.1	12.4		Steel	6.71		.1314	7.81	.675	1.42	2.13	.475	.981	1.436	.108

Projectile Velocity

Two series of experiments were performed to examine the effect of impact velocity on the target crater. These experiments were performed with 356-T51 aluminum targets at 644 K, and columbium - 1 percent zirconium targets at room temperature. All the targets were impacted with 3.18-millimeter diameter spherical Pyrex projectiles of nominally 0.041 gram mass. Figure 1 is a plot of the ratio of the measured penetration depth to projectile diameter as a function of the impact velocity. The penetration is seen to increase with increasing impacting velocity as would be expected.

Hydrodynamic solutions of the semi-infinite impact problem performed by Bjork (ref. 3), Riney and Heyda (ref. 10), and Walsh and Tillotson (ref. 4) gave velocity dependence exponents of 0.33, 0.62, and 0.58, respectively, for impacts of like target and projectile materials. Since these calculations were performed for conditions which apply when the hydrodynamic approximation is valid, they are applicable, strictly speaking, to impact velocities several times the sonic velocity of the material. However, as is generally known, most penetration data at velocities in the neighborhood of
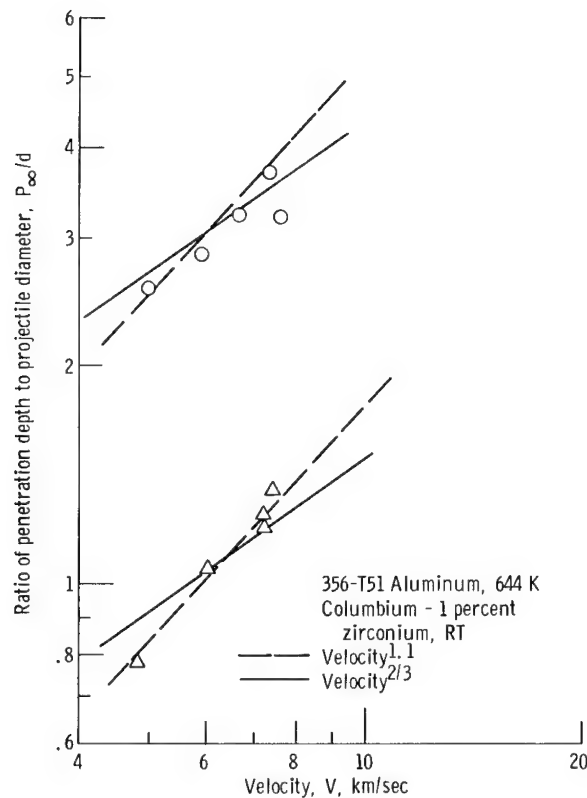
Figure 1. - Penetration as function of impact velocity for
3.18-millimeter-diameter pyrex spheres impacting
356-T51 aluminum at 644 K and columbium - 1 percent
zirconium at room temperature.

the target sonic velocity can be represented by a velocity to the 2/3 power, which is in good agreement with the predictions of Riney and Heyda, and Walsh and Tillotson. Thus, since most of the penetration data presented herein are for velocities slightly higher than the material sonic velocity, a 2/3 power dependence on velocity should be expected.

Shown in figure 1 by the solid lines is a 2/3 velocity dependence for both the aluminum and columbium tested. The dotted line is a 1.1 power velocity dependence. Both variations appear to fit the data equally well. However, because of the few number of data points and the small range of velocity covered, it is not possible to define with precision the velocity dependence variation for these two materials. It is possible with the very few data points presented, that the one low velocity point for each material is weighing the results too heavily. Nevertheless, it can be concluded only that within the range of velocity covered, the velocity dependence could be between 2/3 and 1.1 for the data presented in figure 1.

Projectile Density

The theory of Walsh and Tillotson (ref. 4) predicts no projectile density dependence of damage based on hydrodynamic computations at impact velocities many times the sonic velocity of the target. However, it has been observed experimentally (ref. 12) that the density of the projectile striking a metallic target does have an effect on the extent of the cratering damage produced. This density effect has been estimated to be a 2/3 power dependence from the experiments of reference 12. The impact experiments of reference 12 were performed at velocities that are much lower than those of the theoretical calculations.

The data collected herein for impacts into 316 stainless steel, columbium - 1 percent zirconium, 2024-T6 aluminum alloy and 356-T51 aluminum alloy with Inlyte, nylon, Pyrex, aluminum, and steel projectiles were examined for projectile density effects on crater depth and diameter. The penetration data were normalized with respect to projectile diameter. (Since all impacts were nominally at a constant velocity and projectile masses were nominally the same, no corrections were made to the data to account for the slight differences that did exist.) These data are shown in figure 2. The projectile densities used are those given in table II. In figure 2, lines are drawn for the representation of reference 12 where

$$\frac{P_\infty}{d} \sim \rho_p^{2/3} \tag{1}$$

Although a slightly lower slope is indicated for the 316 stainless steel and columbium - 1 percent zirconium data, the projectile density effect for the materials tested herein
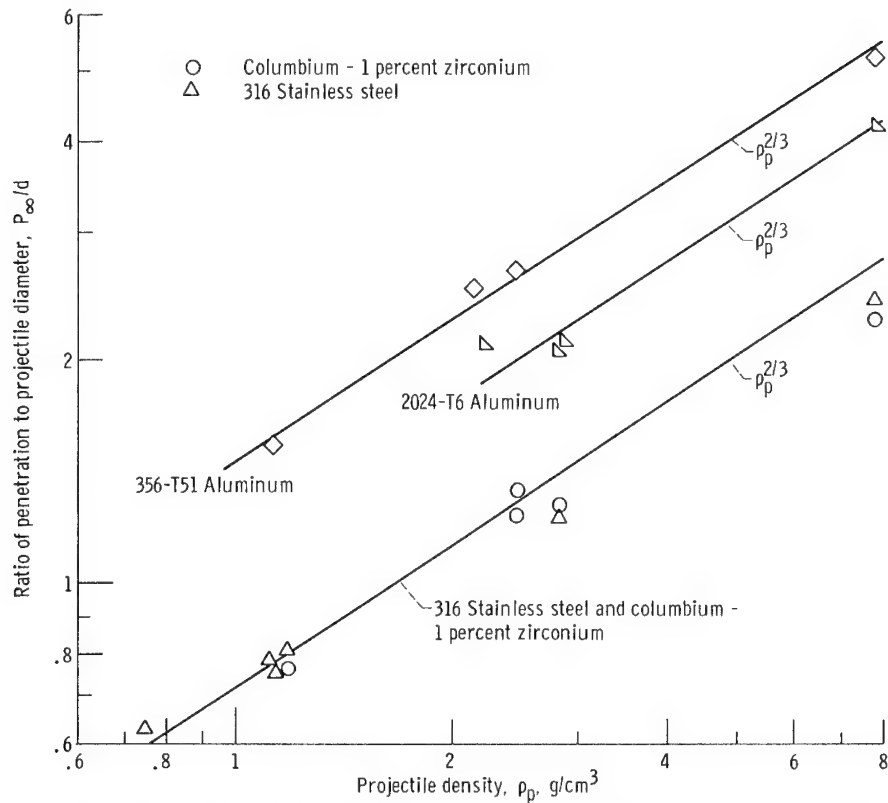
Figure 2. – Penetration as function of projectile density for 3.18-millimeter-diameter spheres impacting at 7.32 kilometers per second (nominal) on 356-T51 and 2024-T6 aluminum, columbium – 1 percent zirconium, and 316 stainless steel at room temperature.
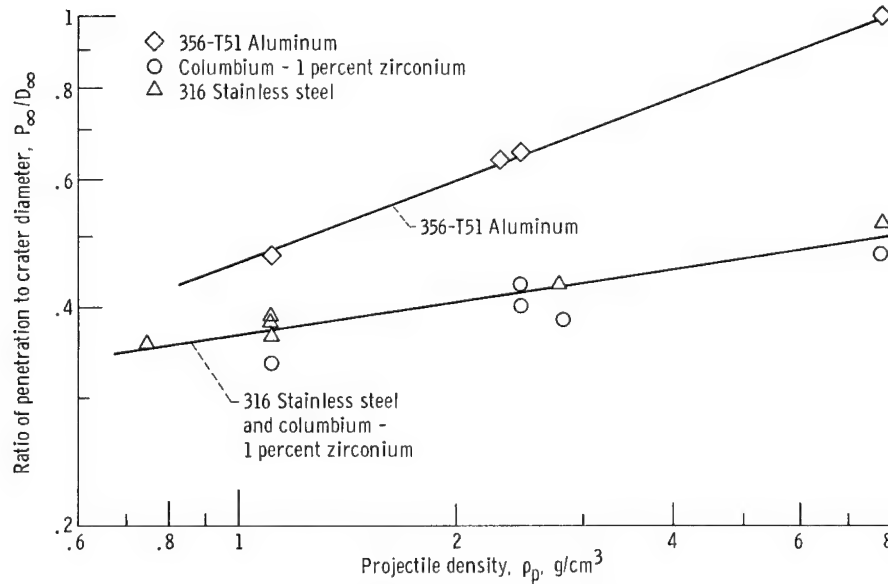

Figure 3. – Ratio of crater depth to crater diameter as function of projectile density for 316 stainless steel, columbium – 1 percent zirconium, and 356-T51 aluminum targets.

10

agrees well with that presented in reference 12.

The hydrodynamic codes of references 3 to 5 and 13 all predict hemispherical craters (ratio of P_∞/D_∞ equal to 0.5) for impacts of projectiles and targets of the same material and for impacts of normal density projectiles into targets of dissimilar materials. As stated previously, the hydrodynamic codes are for velocities many times the sonic velocity and are not, strictly speaking, applicable to the range of velocities obtained in this experimental program. The recent results of Riney in reference 6 for reduced density projectiles predicts a shallower than hemispherical crater for velocities up to 70 kilometers per second.

Figure 3 shows the effect of projectile density on the general shape of the crater. Plotted in the figure is the ratio of penetration depth to crater diameter as a function of projectile density. The data of figure 3 indicate a general increase of the depth to crater diameter ratio with an increase in projectile density. For the steel and columbium targets, the craters are more shallow than hemispherical, whereas the craters are deeper than hemispherical for the cast aluminum targets. The increase in crater depth to crater diameter ratio is more pronounced for the aluminum targets.

Projectile Size

Experiments were performed with two projectile sizes, 3.18 and 2.38 millimeters in diameter. It has been assumed in the previous sections, that the penetration depth and crater diameter scaled directly with projectile size (i.e., P_∞ is directly proportional to projectile diameter). There is strong theoretical support for this assumption (refs. 4, 5, and 10). Nysmith and Denardo (ref. 14), however, have by use of momentum measurements, detected a variation from this rule and have asserted that for the range of projectile sizes tested (1.59 mm to 1.27 cm diameter), penetration is proportional to projectile diameter to the 19/18 power. There has been no explanation as yet given for this difference between the theoretical results and the experimental findings.

Because of the small range in projectile sizes employed herein, and since the observed deviation from direct-size scaling is very small, no attempt was made to check this projectile size effect. (For the range of projectile sizes used in this study, the observed deviations in crater depth should be on the order of three percent, which is well within the experimental accuracy of the tests.)

Target Temperature

Crater formation. - Variations in target temperature in some cases produced large changes in the appearance of the crater, while in others they produced no obvious changes. The most obvious changes occurred with targets of 6061-T6 aluminum and molybdenum. Figure 4 shows the marked change in behavior with the change in temperature in 6061 alloy aluminum. The room temperature impact of this material produced a crater typical of those found in brittle materials; rough crater walls, lack of crater
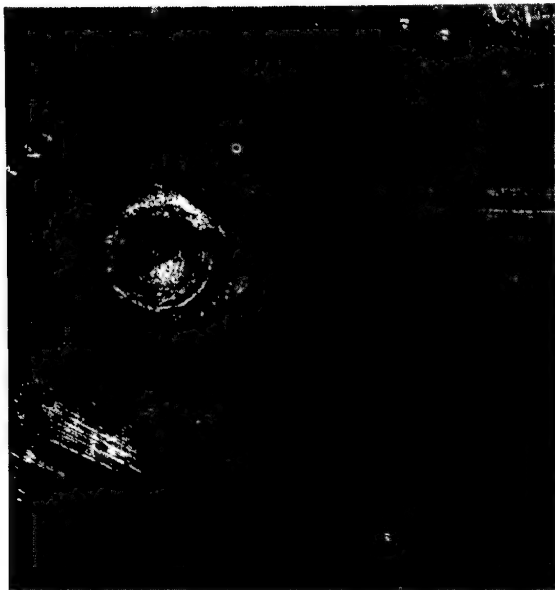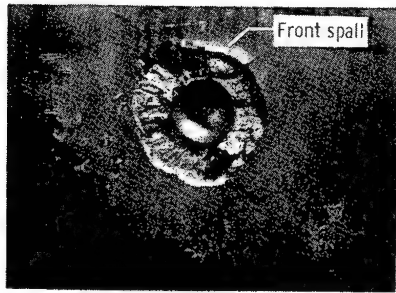

Room temperature.   644 K.

Figure 4. - Targets of 6061-T6 aluminum impacted by 3.18-millimeter-diameter pyrex spheres at room temperature and 644 K.

lips, and front spall surrounding the crater. The same material when impacted at a temperature of 644 K produced a crater more typical of ductile material. The crater walls are smoother, there are lips attached to the crater, and the front spall is no longer in evidence. This same change in character is evidenced in the behavior of molybdenum as shown in figure 5. At room temperature the molybdenum target suffered a large amount of front spall to a distance of about the crater diameter from the crater proper. The same material when impacted at 1365 K (fig. 5) exhibited no front spall and large crater lips. Thus, both the 6061 alloy aluminum and the TZM - molybdenum appear to have gone through a transformation from a brittle fracture behavior at room temperature to a ductile behavior at elevated temperature.
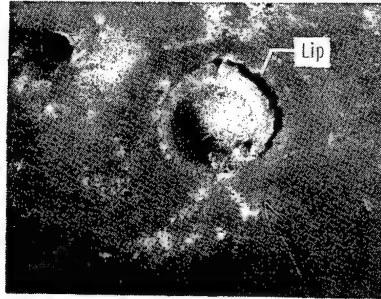
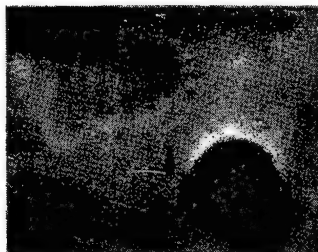Room temperature.   1365 K.   C-68-4346

Figure 5. - Molybdenum targets impacted by 3.18-millimeter-diameter pyrex spheres at room
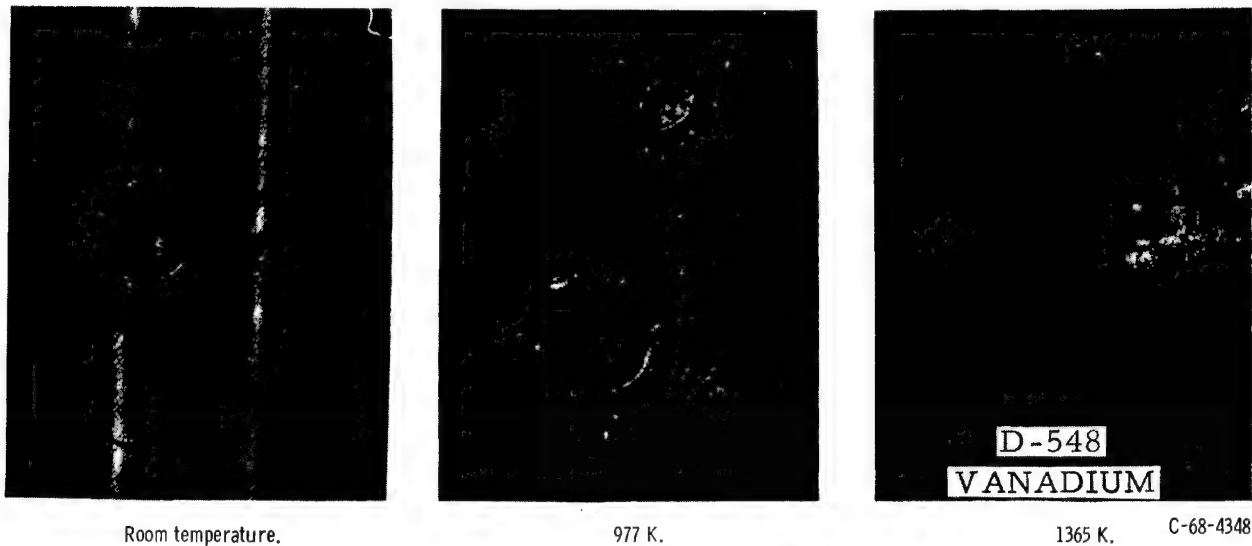temperature and 1365 K.

The L-605 alloy targets shown in figure 6 are typical of materials that exhibited almost no change in crater characteristics when impacted at various target temperatures. At both room temperature and 977 K, the targets are almost identical in appearance; the craters are of the brittle-fracture type with rough crater walls and no crater lips. In figure 7, a series of vanadium targets are shown which also show no marked difference in appearance. The ductile behavior exhibited at room temperature is also present at 977 and 1365 K. In all three targets the crater walls were distinct and smooth, and the craters had large attached lips with no evidence of front spall.

C-68-4347

977 K.

Room temperature.

Figure 6. - Targets of L-605 alloy impacted by 3.18-millimeter-diameter pyrex spheres at
room temperature and 977 K.
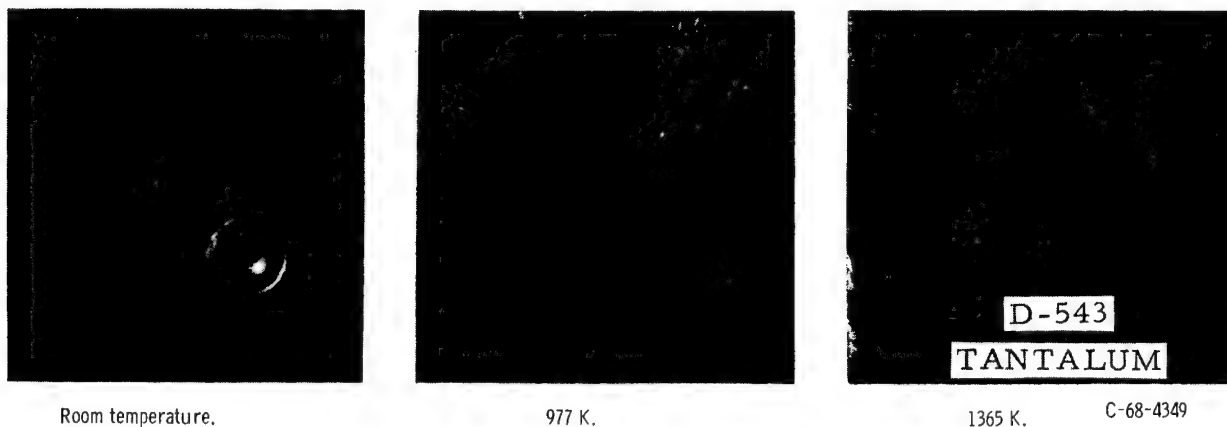
13

Room temperature.   977 K.   1365 K.   C-68-4348

Figure 7. – Vanadium targets impacted by 3.18-millimeter-diameter pyrex spheres at room temperature, 977 K, and 1365 K.

The general tendency for all target materials was from brittle to ductile behavior as the test temperature was increased. The sole exception to this was the behavior of tantalum. As can be seen in figure 8, impacts at room temperature and 977 K into tantalum produced craters with smooth walls and distinct crater lips. When the same material was impacted at 1365 K, the resultant crater had very small crater lips that indicated a more brittle behavior. Close examination of the target showed the surface to be covered with what appeared to be a layer of scale. If the surface was covered with a brittle oxide, this might produce the effect shown in figure 8. In all the experiments, the purity of the helium or nitrogen atmosphere in the impact chamber was not

Room temperature.   977 K.   1365 K.   C-68-4349

Figure 8. – Tantalum targets impacted by 3.18-millimeter-diameter pyrex spheres at room temperature, 977, and 1365 K.
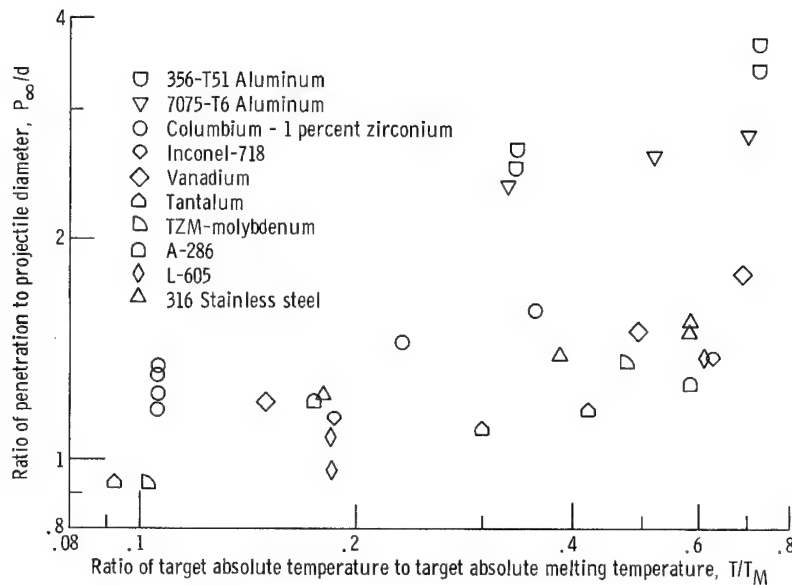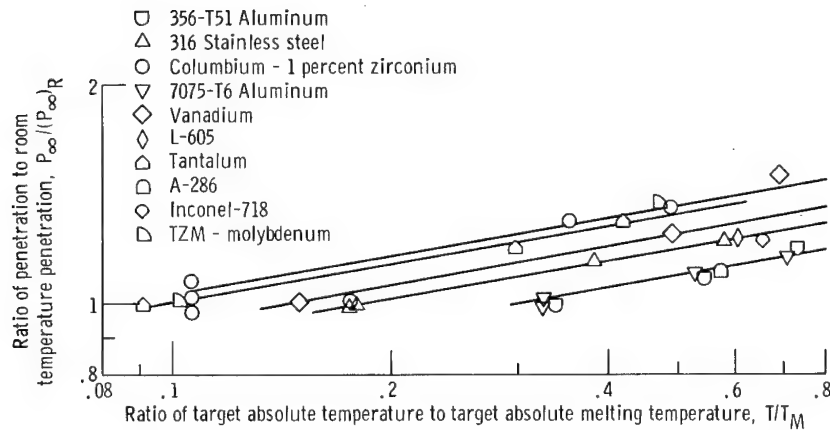
14

Figure 9. – Ratio of penetration depth to projectile diameter as function of target temperature ratio for 3.18-millimeter-diameter pyrex projectiles impacting at 7.32 kilometers per second (nominal).

high, so that some surface oxidation was possible prior to impact.

Data correlation. - The results of the experiments were examined in a more quantitative manner. It was found in every case that an increase in temperature resulted in an increase in penetration, as shown in figure 9. This result is to be expected since it has been found experimentally that target strength plays a role in determining the final crater size (ref. 15), and in general, metals exhibit a reduction in strength with increasing temperature.

In order to compare the results on many materials at various temperatures, the listed absolute test temperatures were normalized with respect to the absolute melting temperature of the material to form the temperature ratio T/T_M. Table IV lists the values of the melting temperature employed for each material. The values are standard handbook values. If a range of melting temperature was provided, the high end of the range was arbitrarily chosen.

In figure 10 the measured depth of penetration divided by the measured room temperature penetration depth is plotted as a function of the absolute temperature ratio T/T_M. The significant part of the figure is the indication that the penetration depths for the materials increase at about the same rate with increasing T/T_M. The lines drawn through each set of data have a slope of 1/6, indicating the possible existence of a temperature correlation of the form

TABLE IV. - MELTING TEMPERATURE OF

TARGET MATERIALS

| Target material	Melting temperature, K
356-T51 Aluminum	886
2024-T6 Aluminum	938
7075-T6 Aluminum	909
Columbium - 1 percent zirconium	2773
Tantalum	3272
TZM - molybdenum	2948
Vanadium	1983
Inconel-718	1590
A-286	1701
316-Stainless steel	1673
L-605	1681

Figure 10. - Ratio of penetration depths as function of target temperature ratio for 3. 18-millimeter-diameter pyrex projectiles impacting at 7. 32 kilometers per second (nominal).

$$\frac{P_\infty}{\left(P_\infty\right)_R} = K_t \left(\frac{T}{T_M}\right)^{1/6} \tag{2}$$

where K_t is some function of the target material, and R refers to room temperature. Specifically, K_t can be determined from the condition that when $T = T_R$, $P_\infty = \left(P_\infty\right)_R$, so that from equation (2)

16

$$K_t = \left(\frac{T_M}{T_R}\right)^{1/6} \qquad (3)$$

Substitution for K_t in equation (2) then yields

$$\frac{P_\infty}{\left(P_\infty\right)_R} = \left(\frac{T}{T_R}\right)^{1/6} \qquad (4)$$

Thus, if the exponent in equation (4) is a representative constant for most materials, the increase in penetration depth at elevated temperatures can readily be obtained from a knowledge of only the room temperature values of penetration depth. This correlation, according to figure 10, appears to be reasonable for values of T/T_M up to about 0.75.

The ratio of the crater depth to crater diameter as a function of the temperature parameter is presented in figure 11. Not much of a correlation is present, except per-
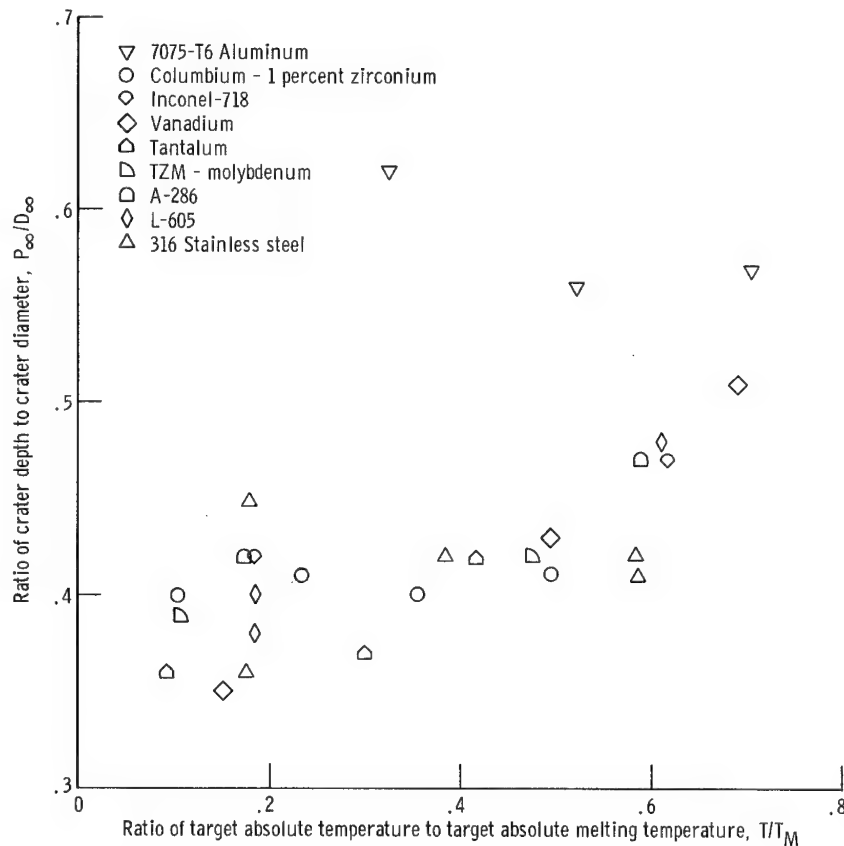
Figure 11. - Ratio of crater depth to crater diameter as function of target temperature for 3.18-millimeter-diameter pyrex projectiles impacting at 7.32 kilometers per second (nominal).

haps, a tendency toward a ratio of $P_\infty/D_\infty = 0.5$ as the temperature increases. This might be expected since as the target temperature increases, the material strength decreases, which tends toward the hydrodynamic condition of no target material strength. As mentioned previously, the hydrodynamic codes predict a hemispherical crater for fully dense projectiles. However, the tendency shown in figure 11 is very slight, and no firm conclusion on crater shape as a function of target temperature can be made.

Cratering Correlation

The estimation of the depth of penetration in a thick (semi-infinite) target due to impact by spherical particles has been made with various empirical equations based on some physical strength property of the material. For example, correlations have appeared based on such target properties as modulus of elasticity, fracture strength, and hardness. Generally, these equations have been developed from data obtained at room temperature. No one approach appears to be superior to the others or to accurately predict crater depth over a wide range of material and impact conditions. This is not surprising when it is considered that the attempt here is to correlate a complex dynamic phenomenon on the basis of a single static property. For practical design use, however, it is desirable to have relatively simple relations in terms of readily available properties.

In order to evaluate the relative effectiveness of various correlation relations, it is necessary to have available a wide variety of impact data and the significant strength and physical properties of the specific targets tested. Unfortunately, the material properties available were inadequate to properly identify the significant strength properties for all of the specific targets tested. Thus, a valid relative comparison of prediction methods could not be made. However, it was possible to select a given correlation approach and develop its specific relation from the test data generated herein. The approach selected was that based on the target modulus of elasticity.

The equation for crater depth based on the target modulus of elasticity is given as (ref. 12)

$$\frac{P_\infty}{d} = \gamma \left(\frac{\rho_p}{\rho_t}\right)^{2/3} \left(\frac{V}{\sqrt{\dfrac{E_t}{\rho_t}}}\right)^{2/3} \tag{5}$$

The 2/3 power dependence for the projectile density has been further confirmed in fig-

18

ure 2. For the velocity exponent, while the limited data of figure 1 did not specifically confirm the 2/3 power variation, they were considered to be inadequate to suggest a revision of the value of the exponent.

Although equation (5) was developed for impacts into various materials at room temperature, it has been applied to elevated temperature impacts, with reliance on the variation of mechanical test values of target modulus with temperature to predict elevated temperature penetration depths (ref. 7). Reference 16 has shown that the use of the equation in this fashion required a variation of the material cratering coefficient γ with temperature. This indicated that the available modulus variations with temperature was insufficient to accurately predict the crater depth at elevated temperature. However, this variability can now be circumvented with the use of equations (4) and (5), room-temperature values of modulus of elasticity, and room temperature values of γ. The use of this approach further eliminates the earlier uncertainty concerning the use of a static or dynamic value of the modulus, since both are generally the same at room temperature.

Combining equations (4) and (5) yields

$$\frac{P_\infty}{d} = \gamma_R \left(\frac{\rho_p}{\rho_t}\right)^{2/3} \left[\frac{V}{\sqrt{\frac{(E_t)_R}{\rho_t}}}\right]^{2/3} \left(\frac{T}{T_R}\right)^{1/6} \tag{6}$$

For equation (6), the determination of γ_R was carried out by plotting the measured values of P_∞/d against the parameter

$$\left(\frac{\rho_p}{\rho_t}\right)^{2/3} \left[\frac{V}{\sqrt{\frac{(E_t)_R}{\rho_t}}}\right]^{2/3} \left(\frac{T}{T_R}\right)^{1/6}$$

where values for target modulus of elasticity $(E_t)_R$ were obtained from unpublished results of a mechanical testing program. These values are listed in table III. Values of target density ρ_t are also given in table III.

The resultant plots for the materials tested are shown in figure 12(a) to (c). Varia-

tions in the parameter of the abscissa for a given material were obtained from variations in projectile density, target temperature, and projectile velocity. The value of room-temperature cratering coefficient γ_R for each material was determined as the slope of the line drawn between the origin and the test data points. The values obtained are listed in table V.

TABLE V. - MATERIAL CRATERING COEFFICIENT

Target material	Material cratering coefficient, γ_R
356-751 Aluminum	2.15
7075-T6 Aluminum	2.00
2024-T6 Aluminum	1.70
Columbium - 1 percent zirconium	1.81
316 stainless steel	2.19
A-286	1.77
Inconel-718	1.85
L-605	2.00
Vanadium	1.71
Tantalum	1.77
TZM - molybdenum	2.00

Comparison of the data points and the straight lines in figure 12 indicates the accuracy of equation (6) in conjunction with the values of γ_R of table V in predicting crater depth in the materials tested over the range of variables covered. If further verified, equation (6) may represent a significant simplification in elevated-temperature cratering predictions, since elevated temperature tests would otherwise have to be conducted for each material and temperature of interest to determine correct values of γ and E_t for use in equation (5).
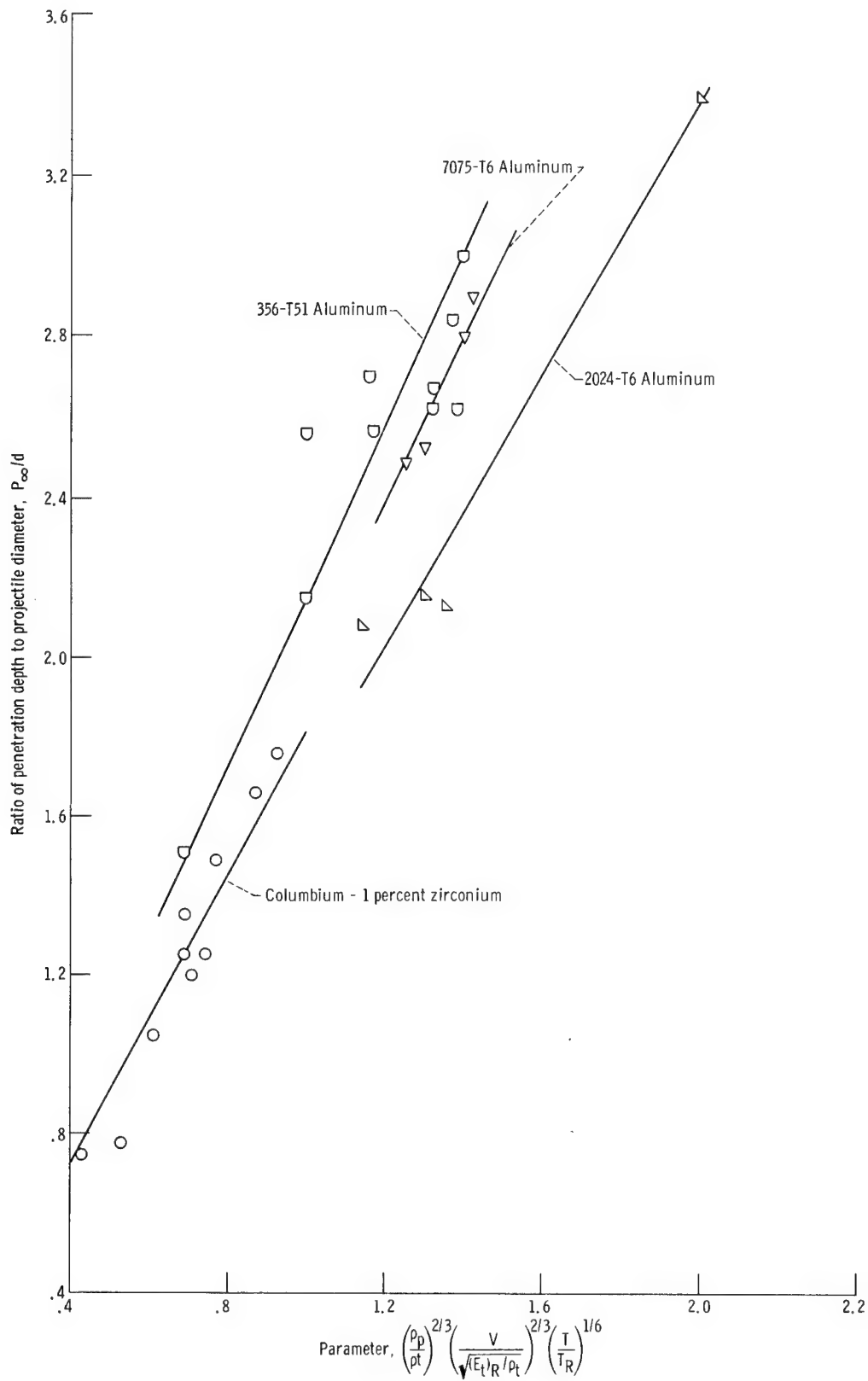
Figure 12. – Correlation of penetration data.
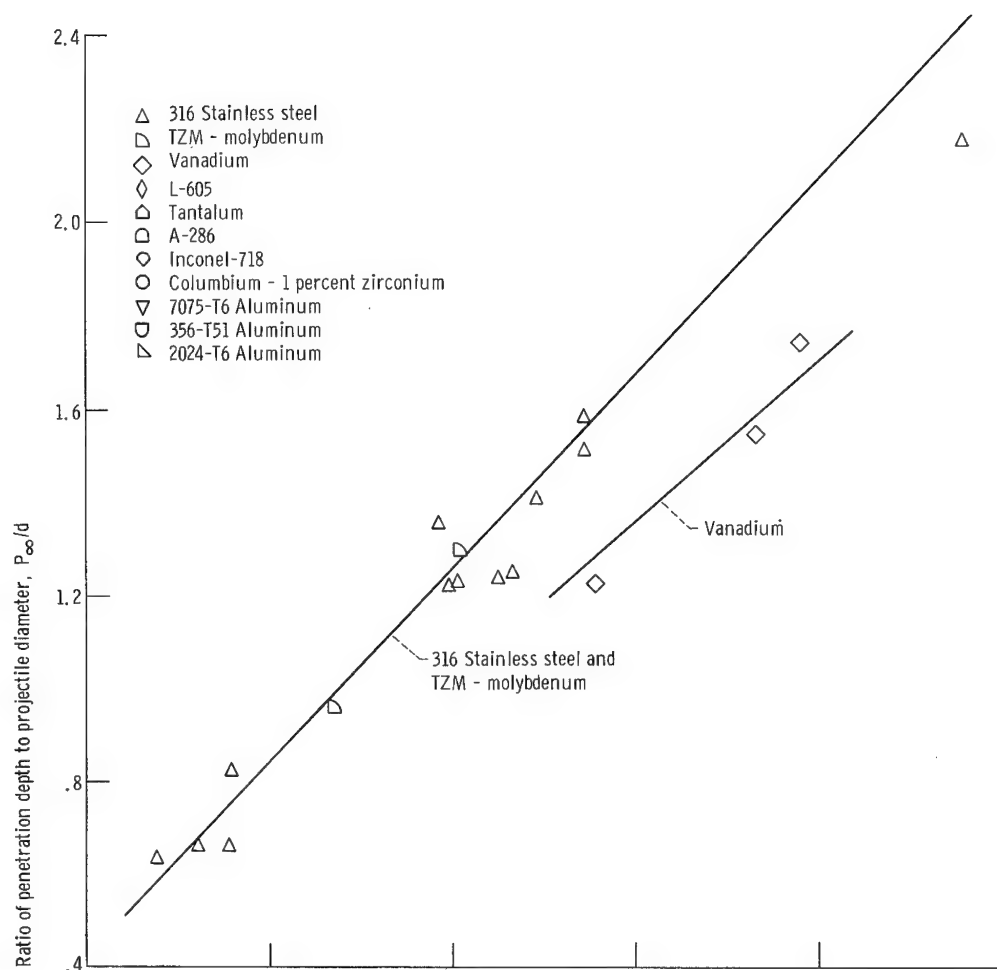
(a) First group.
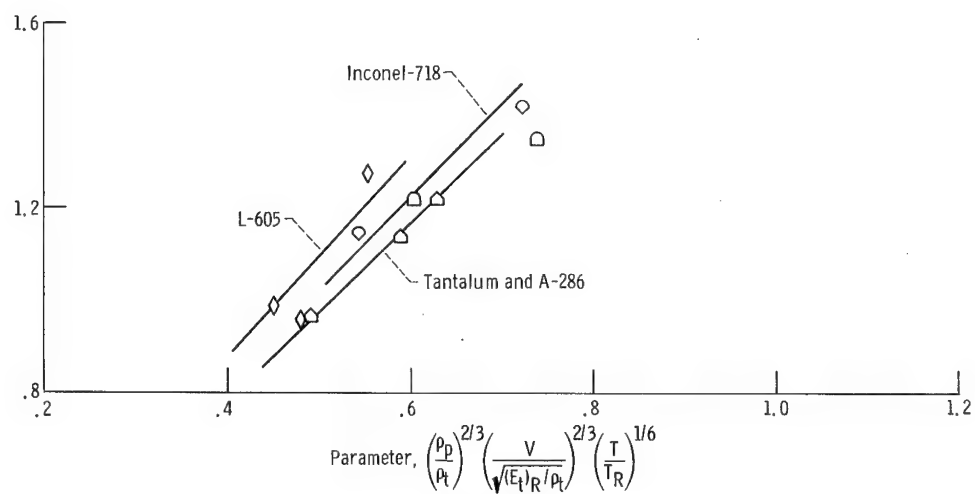
(b) Second group.

Figure 12. – Concluded.

(c) Third group.

SUMMARY OF RESULTS

An experimental research program was conducted to determine the cratering characteristics resulting from the impact of high velocity projectiles in 11 different metal alloys. The major results from this impact program are summarized below.

1. The visually observed damage sustained by the targets was generally characterized as ductile or brittle crater fracture. The materials that generally displayed brittle fracture patterns around the crater from room-temperature impacts with Pyrex projectiles were molybdenum, L-605, Inconel-718, A286, and the 356-T51, 2024-T6, 7075-T6, and 6061-T6 aluminums. Those displaying typically ductile crater fractures at room temperature were vanadium, tantalum, columbium - 1 percent zirconium, and 316 stainless steel.

2. Limited data were obtained on the variation of penetration as a function of impact velocity for 356-T51 aluminum at 644 K and columbium - 1 percent zirconium at room temperature. Because of the small number of data points, no general conclusion on the velocity dependence could be reached for the two materials tested. The penetration depth could vary between 2/3 to 1.1 power of velocity.

3. Tests performed with various projectiles indicated that for a given material, changes in target penetration due to changes in projectile density can be well represented by the penetration being proportional to the 2/3 power of the projectile density.

4. Increasing the temperature of the impacted target above room temperature resulted in an increase in the depth of penetration, which varied as the 1/6 power of the ratio of absolute test temperature to absolute room temperature. Accompanying the increase in penetration depth was a shift to a more ductile behavior of the crater in all materials except tantalum, which appeared to behave in a more brittle fashion at 1365 K than at room temperature.

5. An equation for predicting penetration depths in targets at elevated temperatures has been proposed which requires a knowledge only of modulus of elasticity and a cratering coefficient at room temperature. The various coefficients required for the 11 materials tested are presented for use in the proposed equation.

Lewis Research Center,
   National Aeronautics and Space Administration,
      Cleveland, Ohio, December 23, 1968,
         120-27-04-36-22.

23

APPENDIX - SYMBOLS

D_∞ crater diameter, cm

d projectile diameter, mm

E_t modulus of elasticity, dyne/cm^2

$(E_t)_R$ modulus of elasticity at room temperature, dyne/cm^2

K_t constant

m projectile mass, g

P_∞ semi-infinite penetration depth, cm

$(P_\infty)_R$ semi-infinite penetration depth at room temperature, cm

T target absolute temperature, K

T_M target absolute melting temperature, K

T_R target absolute room temperature, approximately 294 K

V projectile velocity, km/sec

γ material cratering coefficient

γ_R material cratering coefficient at room temperature

ρ_p projectile density, g/cm^3

ρ_t target density, g/cm^3

REFERENCES 74299

1. Whipple, Fred L.: On Meteoroids and Penetration. J. Geophys. Res., vol. 68, no. 17, Sept. 1, 1963, pp. 4929-4939.

2. Clough, Nestor; and Lieblein, Seymour: Significance of Photographic Meteor Data in the Design of Meteoroid Protection for Large Space Vehicles. NASA TN D-2958, 1965.

3. Bjork, R. L.: Effects of a Meteoroid Impact on Steel and Aluminum in Space. Tenth International Astronautical Congress, London, 1959. Vol. 2. Springer-Verlag, 1960, pp. 505-514.

4. Walsh, J. M.; and Tillotson, J. H.: Hydrodynamics of Hypervelocity Impact. Proceedings of the Sixth Symposium on Hypervelocity Impact. Vol. II, Part I. Firestone Tire and Rubber Co., Aug. 1963, pp. 59-104. (Available from DDC as AD-423063.)

5. Riney, T. D.: Visco-Plastic Solution of Hypervelocity Impact Cratering Phenomenon. Proceedings of the Sixth Symposium on Hypervelocity Impact. Vol. II, Part I. Firestone Tire and Rubber Co., Aug. 1963, pp. 105-140. (Available from DDC as AD-423063.)

6. Riney, T. D.; and Heyda, J. F.: Theoretical Prediction of Crater Size for Hypervelocity Impact by Reduced-Density Particles. NASA CR-1196, 1968.

7. Lieblein, Seymour; Clough, Nestor; and McMillan, A. R.: Hypervelocity Impact Damage Characteristics in Armored Space Radiator Tubes. NASA TN D-2472, 1964.

8. Clough, Nestor; McMillan, A. R.; and Lieblein, Seymour: Dimple, Spall, and Perforation Characteristics in Aluminum, Columbium, and Steel Plates Under Hypervelocity Impact. NASA TN D-3468, 1966.

9. Wenzel, A. B.; and Clough, Nestor: Target Pressure and Damage Data From Impacts by Explosively Propelled Projectiles. NASA TM X-1597, 1968.

10. Riney, T. D.; and Heyda, J. F.: Hypervelocity Impact Calculations. Proceedings of the Seventh Hypervelocity Impact Symposium. Vol. II. Martin Co., Feb. 1965, pp. 77-185. (Available from DDC as AD-463228.)

11. Anon.: Aerospace Research Capabilities. Rep. TR63-223, rev., Defense Res. Lab., General Motors Corp., Apr. 1964.

NASA - TN - D 5135

12. Summers, James L.; and Charters, A. C.: High-Speed Impact of Metal Projectiles in Targets of Various Materials. Presented at the Third Hypervelocity Impact Symposium, Armor Res. Foundation, Chicago, Ill., Oct. 7-9, 1958.

13. Walsh, J. M.; and Johnson, W. E.: On the Theory of Hypervelocity Impact. Proceedings of the Seventh Hypervelocity Impact Symposium. Vol. II. Martin Co., Feb. 1965, pp. 1-75. (Available from DDC as AD-463228.)

14. Denardo, B. Pat; and Nysmith, C. Robert: Momentum Transfer and Cratering Phenomena Associated with the Impact of Aluminum Spheres into Thick Aluminum Targets at Velocities to 24,000 feet per Second. The Fluid Dynamic Aspects of Space Flight. Vol. 1. AGARDograph-87, Vol. 1. Gordon and Breach Science Publ., 1966, pp. 389-402.

15. Kineke, J. H.; and Richards. L. G.: Influence of Target Strength on Hypervelocity Crater Formation in Aluminum. Proceedings of the Sixth Hypervelocity Impact Symposium. Vol. II, Pt. 2. Colorado School of Mines, Aug. 1963, pp. 513-524.

16. Clough, Nestor; Diedrich, James H.; and Lieblein, Seymour: Results of Hypervelocity Impacts into Space Radiator Materials. Presented at the AIAA First Rankine Cycle Space Power Systems Specialists Conference, Cleveland, Oct. 26-28, 1965.

"The aeronautical and space activities of the United States shall be conducted so as to contribute . . . to the expansion of human knowledge of phenomena in the atmosphere and space. The Administration shall provide for the widest practicable and appropriate dissemination of information concerning its activities and the results thereof."

— NATIONAL AERONAUTICS AND SPACE ACT OF 1958

NASA SCIENTIFIC AND TECHNICAL PUBLICATIONS

TECHNICAL REPORTS: Scientific and technical information considered important, complete, and a lasting contribution to existing knowledge.

TECHNICAL NOTES: Information less broad in scope but nevertheless of importance as a contribution to existing knowledge.

TECHNICAL MEMORANDUMS: Information receiving limited distribution because of preliminary data, security classification, or other reasons.

CONTRACTOR REPORTS: Scientific and technical information generated under a NASA contract or grant and considered an important contribution to existing knowledge.

TECHNICAL TRANSLATIONS: Information published in a foreign language considered to merit NASA distribution in English.

SPECIAL PUBLICATIONS: Information derived from or of value to NASA activities. Publications include conference proceedings, monographs, data compilations, handbooks, sourcebooks, and special bibliographies.

TECHNOLOGY UTILIZATION PUBLICATIONS: Information on technology used by NASA that may be of particular interest in commercial and other non-aerospace applications. Publications include Tech Briefs, Technology Utilization Reports and Notes, and Technology Surveys.

Details on the availability of these publications may be obtained from:

SCIENTIFIC AND TECHNICAL INFORMATION DIVISION

NATIONAL AERONAUTICS AND SPACE ADMINISTRATION
Washington, D.C. 20546